

# Study on Ultra-high Electro-Magnetic Flux Generation using LS-DYNA<sup>®</sup> Multi-Physics Capability

Kunio Takekoshi

*Terrabyte Co., Ltd.*

*NOV Bldg. 3F, Yushima 3-10-7, Bunkyo-ku, Tokyo, 113-0034, Japan*

## Abstract

*Simulation results about two kinds of Electro-Magnetic Flux Generation Methods using LS-DYNA Multi-Physics capability are reported in this paper. It is revealed that the Burgess Model should be considered to model electrical conductivity as functions of relative volume as well as temperature, and that hourglass control type 6 should be used in order to precisely predict the generation of magnetic flux density and the deformation of coil for the methods.*

## Introduction

It is challenging to predict dynamical process of deformation of a coil and generation of magnetic flux density in the Electro-Magnetic Flux Generation Methods, since the methods involve complex physics like hi-speed deformation, electro-magnetic forming, material properties as functions of temperature and relative volume, and phase transition between solid, liquid and gas phases. LS-DYNA offers us electromagnetism solver as well as sophisticated mechanical solver and thermal solver since the release of version R7. Therefore the Electro-Magnetic Flux Generation Methods can be good benchmark problems for LS-DYNA multi-physics capability.

This study is the second report about the Electro-Magnetic Flux Generation Method using LS-DYNA multi-physics capability from the Ref. [1] and reveals the importance of the electrical conductivity and hourglass control in the simulation of the Electro-Magnetic Flux Generation.

## Ultra-High Electro-Magnetic Flux Generation

The purpose of the ultra-high electro-magnetic flux generation is to investigate electronic property of materials such as carbon nano-tubes utilizing the nature that the spin and orbital motion of electrons are precisely controlled by magnetic field. This is because the technique can generate the ultra-high magnetic flux density over several hundred Tesla, and novel electronic behaviors of materials excited by the ultra-high magnetic field are expected to be observed.

There are several methods of the ultra-high electro-magnetic flux generation. In this study, two methods, (1) Electro-Magnetic Flux Compression (EMFC) Method [2, 3, 4], and (2) Single Turn Coil (STC) Method [5, 6] are studied using LS-DYNA.

**Method 1: Electro-Magnetic Flux Compression (EMFC)**

Fig. 1 shows main parts of the EMFC method based on the system developed by UTokyo International Megagauss Science Laboratory [2, 3, 4]. There are four coils, a liner coil, a primary coil, a support coil, and a set of Helmholtz coil. A specimen is set at the center of the liner coil during measurement. The procedure of the Electro-Magnetic Flux Compression was described in Ref. [1].

**Method 2: Single Turn Coil (STC)**

Fig. 2 shows a main part of the STC method based on the system operated by UTokyo International Megagauss Science Laboratory [5, 6]. A specimen is set at the center of the coil during measurement. Magnetic flux density is generated injecting a large electric current 2 MA into the coil within 10  $\mu$ sec before the coil is broken due to repulsive Lorentz force directed outside of the coil. As a result, the maximum value of the magnetic flux density generated at the center of the coil achieves around 300 T.

The advantage of this method is that a specimen located at the center of the coil is not crushed after the generation of the electro-magnetic flux, because the coil is burst out, not imploded. Therefore, researchers can confirm reproducibility of their measurement result for the same specimen.

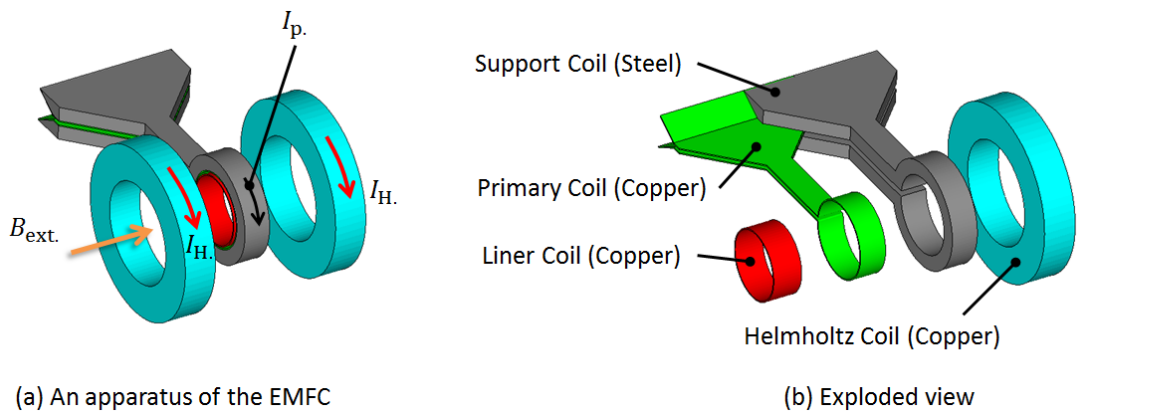


Fig. 1. The Electro-Magnetic Flux Compression (EMFC) system developed by Takeyama et al., UTokyo International Megagauss Science Laboratory [2, 3, 4].

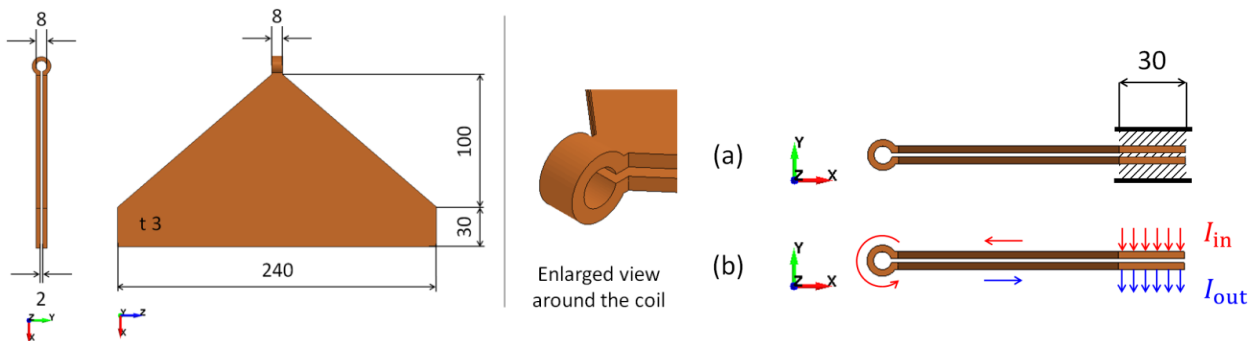


Fig. 2. (Left) The Single Turn Coil (STC) employed by UTokyo International Megagauss Science Laboratory [5, 6] (Right, a) Boundary condition of the coil fixed by clamping system. (Right, b) Locations of the electric current input and output.

## Simulation Models

Simulation models for the two methods are developed based on the UTokyo systems as shown in Fig. 1 and Fig. 2. These simulation models are composed of hexahedral elements with one integration point (ELFORM=1) so that large deformation of coils and eddy current distribution can be precisely simulated.

Hourglass control for these models is type 6 with its coefficient 2.0 rather than the type 5 with its coefficient 0.05 which is widely used for metal materials. The effect of hourglass control on the simulation results is discussed later.

Simulation time for the EMFC model is 20.050 msec, 20 msec for the development of external magnetic field and 50  $\mu$ sec for the electromagnetic compression phase. Simulation time for the STC model is 6  $\mu$ sec.

### Constitutive Material Models and Its Parameters

Materials for the components and corresponding constitutive model for the structural solver used in this study are listed in Table 1.

For the EMFC model, the liner and primary coils are modelled using tabulated Johnson-Cook model (\*MAT\_224) which can consider temperature dependent Young's modulus. The support and the Helmholtz coils are modelled using Johnson-Cook model (\*MAT\_015) and rigid model (\*MAT\_020), respectively, because the support and Helmholtz coils are not of interest in this study.

For the STC model, the coil is also modelled using tabulated Johnson-Cook model with the same parameter used in the EMFC model.

Table 1. Components, material, and corresponding constitutive model for the Electro Magnetic Flux Compression System in this study.

Component	Material	Constitutive model	EOS	Constants
Liner Coil	Copper	Johnson-Cook [7]	Gruneisen	Ref. [8, 9]
Primary Coil	Copper	Johnson-Cook	Gruneisen	Ref. [8, 9]
Support Coil	Steel	Johnson-Cook	Gruneisen	Ref. [10]
Helmholtz Coil	Copper	Rigid	-	-
Single Turn Coil	Copper	Johnson-Cook	Gruneisen	Ref. [8, 9]

Materials for the components and corresponding EOS model of electrical conductivity for the electromagnetism solver used in this study are listed in Table 2.

For the EMFC model, the liner and primary coils are modelled using the Burgess Model [11] considering temperature and relative volume dependences above the melting point. The support coil is modelled using tabulated EOS considering electrical conductivity as a function of temperature. Electrical conductivity for the Helmholtz coil in this study is not needed, since the imposed current injected into the Helmholtz Coil is controlled by \*EM\_CIRCUIT\_SOURCE where the electric current will be considered uniform.

For the STC model, the coil is also modelled using the Burgess Model.

Table 2. Components, material, and corresponding EOS of conductivity in this study.

Component	Material	EOS	Constants
Liner Coil	Copper	Burgess Model [11]	Ref. [11]
Primary Coil	Copper	Burgess Model	Ref. [11]
Support Coil	Steel	Tabulated Data	Ref. [12]
Helmholtz Coil	Copper	-	-
Single Turn Coil	Copper	Burgess Model	Ref. [11]

Material constants used by thermal solver are determined by references [8, 13] for copper, and by references [10, 13] for steel. In this study, temperature dependence of thermal conductivity and specific heat for the liner coil (copper), the primary coil (copper) and the support coil (steel) are considered using \*MAT\_THERMAL\_ISOTROPIC\_TD\_LC.

### Boundary Condition and Miscellaneous

Boundary condition for the EMFC model was described in Ref. [1] and that for the STC model is shown in Fig. 2. These locations are clamped during measurements.

Input electric current for the EMFC model was also described in Ref. [1] and that for the STC model is an experimentally obtained data in Ref. [5].

These two simulation models are analyzed using a development version of MPP-DYNA (SVN Revision 105651), with 28 CPU cores on a Linux cluster.

## Simulation Results

### Method1: Electro-Magnetic Flux Compression

Fig. 3 shows a comparison about dynamical process of the liner coil implosion between the simulation result of the EMFC model and a typical experimental result [14, 15]. The imploding process of the liner coil is qualitatively simulated, although the time stamp between the two results differs. In order to compare these two results, the time stamp of selected snap shots in the simulation result is chosen using a formula  $t_{\text{final step}}^{\text{sim.}} \cdot t^{\text{exp.}} / t_{\text{final step}}^{\text{exp.}}$ , here the upper suffixes “sim.” and “exp.” represent abbreviation of simulation and experiment, respectively.

Another remarkable result in Fig. 3 is asymmetric deformation of the liner coil with respect to the vertical due to non-uniform magnetic field caused by the gap of primary coil. In the simulation result, this asymmetric deformation is seen after 34.0  $\mu\text{sec}$ , while in the experimental result, the deformation was slightly seen after 34.8  $\mu\text{sec}$ . In addition, a flash at the left side of the liner coil at 39.8  $\mu\text{sec}$  was observed, indicating that short circuit inside of the liner coil was occurred as the result of asymmetric deformation.

Fig. 4 also shows a comparison about the inner diameter of the liner coil as a function of magnetic flux density  $B_z$  between the simulation result of the EMFC model and the experimental result [3, 4]. The simulation model successfully predicts the experimental result, especially above 200 Tesla.

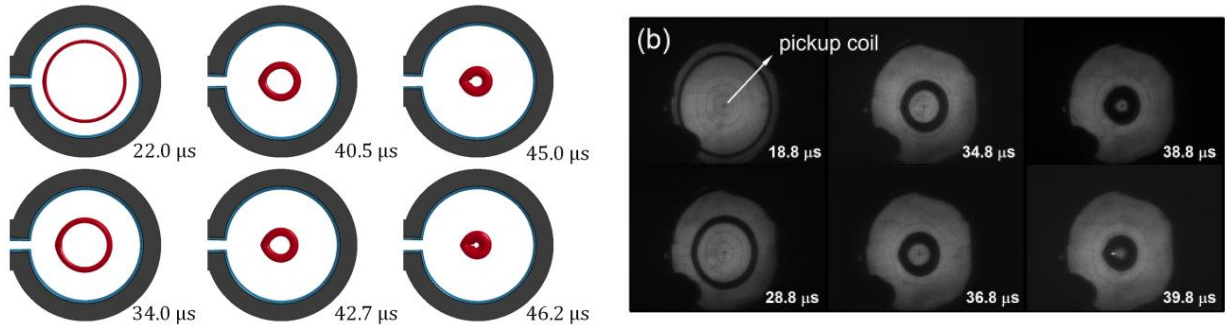


Fig. 3. (Left) Evolution of liner coil predicted by the electro-magnetic flux compression simulation. (Right) A typical shadowgraph of the imploding liner [14, 15].

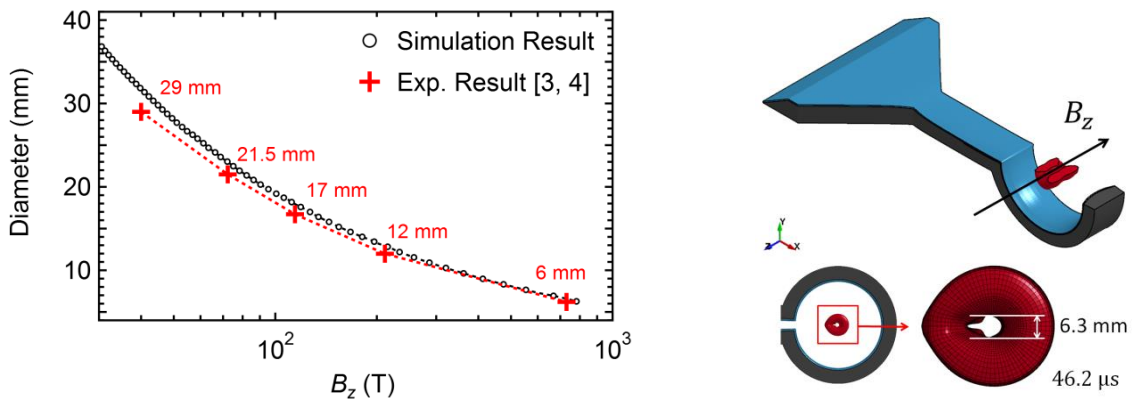


Fig. 4. (Left) Diameter of the liner coil as a function of magnetic flux density  $B_z$  at the center of the liner coil. (Right top) The direction of magnetic flux density  $B_z$ . (Right bottom) Example of evaluating the inner diameter of the liner coil at 46.2  $\mu$ sec.

**Method2: Single Turn Coil**

Fig. 5 shows a comparison about magnetic flux density  $B_z$  generated at the center of the coil as a function of time in the STC method between the simulation result and the experimental result. The simulation stops around 3.2  $\mu$ sec because electromagnetism solver does not return to main routine. This may be because there are some distorted elements around the coil. Although the simulation model cannot predict whole experimental result, it successfully predicts the time history of magnetic flux density until 3.2  $\mu$ sec.

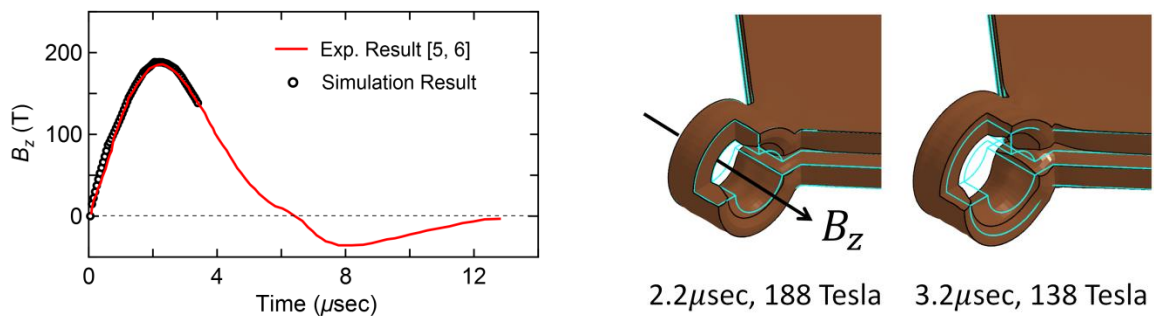


Fig. 5. (Left) A comparison of magnetic flux density  $B_z$  generated at the center of the coil in the Single Turn Coil between the simulation result and the experimental result [5, 6]. (Right) Deformation of the Single Turn Coil at different time. Light blue lines represent the initial shape of the Single Turn Coil. An arrow represents the direction of  $B_z$ .

## Discussion

First report of the simulation result of the EMFC method was given in Ref. [1] where the simulation successfully predicted the inner diameter of the liner coil as a function of magnetic flux density below 100 Tesla while the simulation underestimated it above 100 Tesla. A question arises what is important in predicting the experimental result. Let us consider electrical conductivity and hourglass control, because these two things in this study are different from those in the previous one.

### The electrical conductivity

Fig. 6 shows electrical conductivity for copper as functions of temperature and the relative volume. The dashed lines represent electrical conductivity governed by the Burgess model [11], and the open circle represents the recommended value based on many experimental reports compiled by Matula [16]. In the previous simulation result, the data from Matula was employed to simulate the EMFC method. Although both data have qualitatively the same electrical conductivity above and below the melting point, the data from Matula is available below 1700 K. This value 1700 K is not enough, because a part of the liner coil is subjected to liquid and gas phases during measurement, and boiling point is about 2835 K.

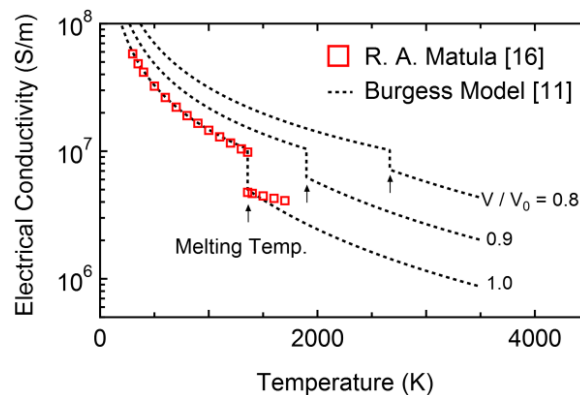


Fig. 6. Electrical conductivity as functions of temperature and relative volume  $V/V_0$  where  $V_0$  is the reference specific volume under zero pressure (solid phase).

The data from Matula is considered not enough to simulate the liner imploding process because of following two reasons; (1) the imploding process involves solid-liquid-gas phase transition during measurement as mentioned above, (2) the liner coil is extremely compressed. In order to solve the problem regarding the first reason, it is necessary to consider electrical conductivity as a function of wide range of temperature, and the Burgess Model gives us its solution.

As for the second reason, it is well known that melting and boiling points for a typical material except water are shifted higher with increasing pressure. Here, let us investigate volumetric strain of the coil instead of pressure. Fig. 7 shows a contour plot of the volumetric strain for the liner coil. The volumetric strain around the inner region of the coil below 200 Tesla is within  $\pm 5\%$ . However the strain in the vicinity of the center of the coil at 780 Tesla reaches

around  $-10\%$ . Under the compression state of stress, the melting point for copper material shifts higher temperature and electrical conductivity results in higher value according to the Burgess Model, indicating that eddy current on the inside surface of the coil modelled by the Burgess Model easily flows as compared with that modelled by the Matura's data.

Burgess Model is also important in simulating the STC method. When the STC model employs the data from Matura, the calculation stops  $1.2\ \mu\text{sec}$  due to the convergence error of electromagnetism FEM-BEM solver. The reason is presumably for that the temperature around the coil reaches beyond 2000 K and the appropriate electrical conductivity is not given.

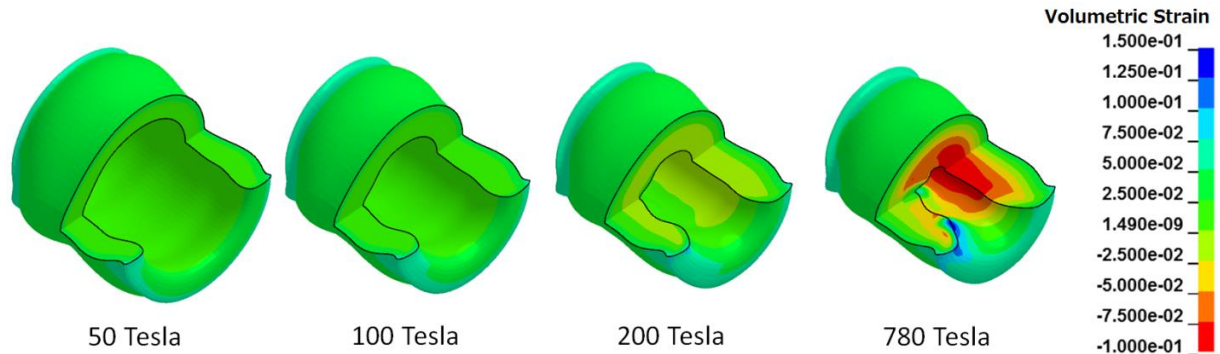


Fig. 7. Contour plot of volumetric strain for the liner coil as a function imploding process and magnetic flux density generated at the center of the coil.

### The hourglass control

Fig. 8 shows a comparison about the spatial dependence of magnetic flux density (intensity) at different times between the experimental result [14, 17] and two simulation results in order to investigate effect of the hourglass control. Two simulation results are obtained using the same EMFC model except for the hourglass control. The center and right graphs in Fig. 8 come from the simulation models using hourglass type 6 with its coefficient 2.00 (HG=6) and using hourglass type 5 with its coefficient 0.10 (HG=5), respectively.

Both simulation results drastically differ from each other as shown in Fig. 8. For the low level of magnetic flux density, the simulation result for the HG=5 predicts a characteristic hump around 10 mm in coil axis, while for the high level of magnetic flux density, the result for the HG=6 shows a single peak around 0 mm in coil axis and a shoulder around 12.0 mm. In addition, it is interesting that the single peak gradually develops from 43.0 to 46.3  $\mu\text{sec}$ , and the same kind of development of the single peak is also seen from 39.2 to 40.1  $\mu\text{sec}$  in the experimental result.

Fig. 9 shows a comparison about electrical current density on the surface of the liner coil between two simulation results, HG=6 and HG=5. Development of a characteristic hump at the vertical center of the liner coil and two small humps (11.5 mm) are observed from 100 to 780 Tesla for the HG=6 result, while development of two characteristic humps (9.1 mm) are observed from 100 to 520 Tesla for the HG=5 result. Since high electrical current density flows near the humps for both results, it is reasonable to consider that these humps correspond to the development of magnetic flux density  $B_z$ , the single peak and the shoulder for the HG=6 result and the hump, shown in Fig. 8.

The development of the single peak is important in predicting the inner diameter of the liner coil as a function of magnetic flux density above 200 Tesla. Fig. 10 shows another comparison between the simulation results for HG=6 and HG=5. The underestimation of  $B_z$  found in HG=5 corresponds to failure of development of the single peak around 0 mm in coil

axis from time stamp 45.4  $\mu$ sec to 46.2  $\mu$ sec shown in Fig. 8. This underestimation can be understood using the Biot-Savart law as shown in Eq. 1,

$$\Delta B = \frac{\mu_0}{4\pi} \frac{I \Delta s \times r}{r^3} \tag{Eq. 1}$$

, where  $I \Delta s$  is current segment vector,  $r$  is distance between an evaluation point and location of the current segment. According to the law, magnetic flux density  $B_z$  is drastically decreased by  $r^2$  with increasing the distance  $r$ . Distances from locations of large current density shown by two arrows for HG=5 are larger than distances shown by an arrow at the vertical center for HG=6, corresponding to the underestimation of  $B_z$  at the location #0.

In other words, development of the single peak is essential in predicting the generation of magnetic flux density by the EMFC method. Therefore the choice of the hourglass control is important. In this simulation, hourglass type 6 with its coefficient 2.00 is very effective, although the coefficient value is very high as compared with the coefficient used by many simulations according to the LS-DYNA User’s Manual.

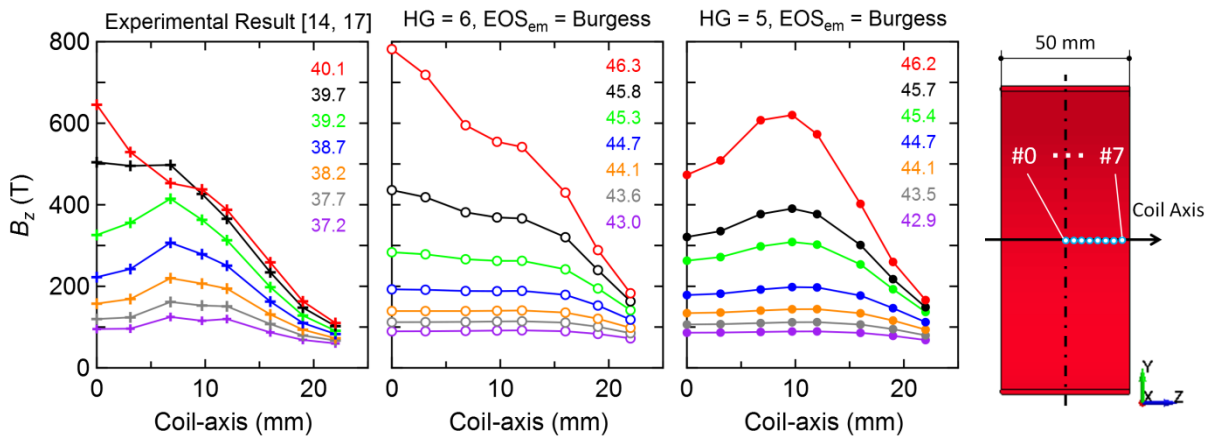


Fig. 8. Spatial dependence of magnetic flux density (intensity) at different times obtained by an experiment [14, 17] and the simulation considered in this study. These data points are evaluated at each location #0 ~ #7 along with the coil axis shown in right figure.

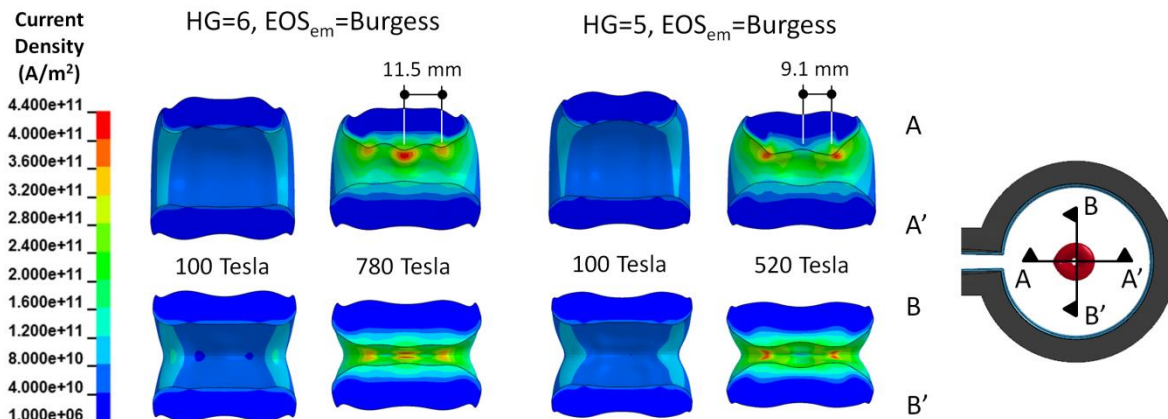


Fig. 9. Contour plot of electrical current density on the surface of the liner coil for the simulation results, HG=6 and HG=5.

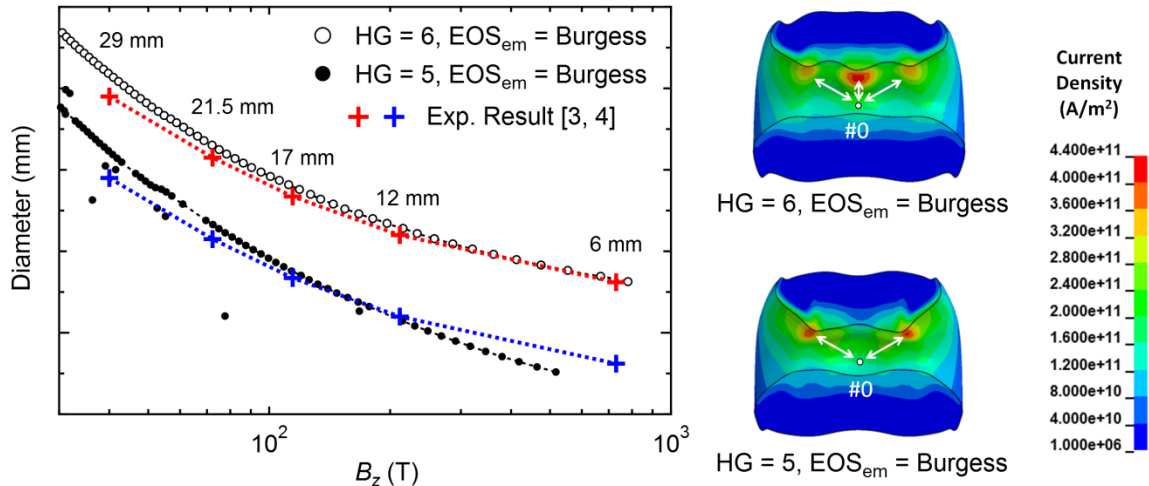


Fig. 10. A comparison about the inner diameter of the liner coil as a function of magnetic flux density  $B_z$  between two simulation results (open and close circles) and the experimental result (red and blue cross) [3, 4]. Contour plot of current density on the surface and cross section of the liner coil for the two simulation results, HG=6 and HG=5.

### Miscellaneous

Electrical circuits including resistors, capacitances and inductances are not considered in the two simulation models in this study. However, it is necessary to consider electrical circuits in simulating the Electro-Magnetic Flux Generation methods before experiments. Therefore the simulation models have to be upgraded to include electrical circuits in future study.

There is an unresolved issue “turn around behavior” in the simulation of the EMFC method. In experiments, magnetic flux density reaches peak value around 700 Tesla and then decreases. This behavior is called “turn-around behavior”. Currently, the reason is not found why the turn-around behavior is not observed in the simulation results presented here.

Mechanical properties considering phase transition between solid and liquid phases are not employed in this study, although the electrical conductivity considering phase transition is employed. In order to incorporate the effect of the phase transition in the mechanical solver, GRAY EOS [18] needs to be implemented through user subroutine [19]. It is interesting if the GRAY EOS explains the turn-around behavior in the EMFC method.

### Conclusion

It is found that the Burgess Model should be considered to model electrical conductivity for metal material as functions of temperature and relative volume, and that hourglass control type 6 should be used rather than type 5 for metal materials in the simulation of the Electro-Magnetic Flux Generation.

## Acknowledgement

The author thanks for helpful support by Dr. Pierre L'Eplattenier and Dr. Inaki Caldichoury, LSTC. They implemented some features of the electro-magnetism solver for this study. The author also thanks for helpful discussion with Professor Shojiro Takeyama and Dr. Daisuke Nakamura, UTokyo International MegaGauss Science Laboratory. They provided experimental results and showed detailed setup of their experimental apparatus.

## References

- [1] K. Takekoshi, "Simulation of the Electromagnetic Flux Compression using LS-DYNA Multi-Physics Capability," *Proceedings of the 10th European LS-DYNA Conference 2015*, 2015.
- [2] S. Takeyama, "The World Highest Magnetic Field as Indoor Generation and Its Application to Solid State Physics," *The Physical Society of Japan*, vol. 67, no. 3, p. 170, 2012.
- [3] S. Takeyama and E. Kojima, "A copper lined magnet coil with maximum field of 700 T for electromagnetic flux compression," *Journal of Physics D: Applied Physics*, vol. 44, p. 425003, 2011.
- [4] S. Takeyama, S. Hironobu and K. Eiji, "Recent Developments of the Electro-Magnetic Flux Compression," *Journal of Low Temperature Physics*, vol. 159, pp. 328-331, 2010.
- [5] N. Miura, "Solid state physics in megagauss fields generated by electromagnetic flux compression and single-turn coils," *Physica B*, vol. 201, pp. 40-48, 1994.
- [6] K. Nakao, F. Herlach, T. Goto, S. Takeyama, T. Sakakibara and N. Miura, "A laboratory instrument for generating magnetic fields over 200 T with single turn coils," *J. Phys. E: Sci. Instrum.*, vol. 18, pp. 1018-1026, 1985.
- [7] G. R. Johnson and W. H. Cook, "A constitutive model and data for metals subjected to large strains, high strain rates and high temperatures.," *Proc. 7th Int. Symposium on Ballistics.*, pp. 541-547, 1983.
- [8] B. Banerjee, "An evaluation of plastic flow stress models for the simulation of high-temperature and high-strain-rate deformation of metals," *cond-mat*, p. 0512466v1, 2005.
- [9] H. M. Ledbetter and E. R. Naimon, "Elastic Properties of Metals and Alloys. II. Copper," *J. Phys. Chem. Ref. Data*, vol. 3, no. 4, pp. 897-935, 1974.
- [10] B. Banerjee, "The Mechanical Threshold Stress model for various tempers of AISI 4340 steel," *cond-mat*, p. 0510330v1, 2005.
- [11] T. J. Burgess, "Electrical resistivity model of metals," *4th International Conference on Megagauss Magnetic-Field Generation and Related Topics, Santa Fe, NM, USA*, 1986.
- [12] Japan Society of Thermophysical Properties, *Thermophysical Properties Handbook*, YOKENDO, 2008
- [13] R. W. Powel, C. Y. Ho and P. E. Liley, "Thermal Conductivity of Selected Materials," *National Standard Reference Data Series - National Bureau of Standards - 8*, 1966.
- [14] D. Nakamura, H. Sawabe, Y. H. Matsuda and S. Takeyama, "Dynamical Process of Liner Implosion in the Electromagnetic Flux Compression for Ultra-high Magnetic Fields," *arXiv*, p. 1309.1038, 2013.
- [15] *Photos are presented from the International Megagauss Science Laboratory, the ISSP, Univ. of Tokyo by their courtesy.*
- [16] R. A. Matula, "Electrical Resistivity of Copper, Gold, Palladium, and Silver," *J. Phys. Chem. Ref. Data*, vol. 8, no. 4, p. 1147, 1979.
- [17] D. Nakamura, H. Sawabe and S. Takeyama, "Note: Experimental evidence of three-dimensional dynamics of an electromagnetically imploded liner," *Review of Scientific Instruments*, vol. 036102, p. 85, 2014.
- [18] Royce. E.B, "UCRL-51121 - GRAY, A THREE-PHASE EQUATION OF STATE FOR METALS," *LLNL*, Vols. September, 3, 1971.
- [19] L. B. Gael, J. Petit, P.-Y. Chanal, L. Pierre and A. Gilles, "Modelling the dynamic magneto-thermomechanical behaviour of materials using a multi-phase EOS," *the proceedings of 7th European LS-DYNA Conference*, pp. C-II-04, 2009.